Atomic K-shell excitation at ultrarelativistic impact energies

Allan H. Sørensen*
Organisation Européenne pour la Recherche Nucléaire (CERN), CH-1211 Genève 23, Switzerland
(Received 5 February 1987; revised manuscript received 18 May 1987)

After ten years of nonsuccessful experimental searches for a "density effect" in inner-shell excitation, a recent experiment has shown pronounced moderation—although not full saturation—in K-vacancy production in aluminum and copper foils at ultrarelativistic impact energies. In the present paper a comprehensive theoretical investigation of atomic K-shell excitation by charged GeV projectiles is presented with special emphasis on the influence of target polarization. The gradual onset of polarization and "transition radiation" emitted near the target incidence surface is shown to compensate partly the reduction due to the density effect. Inner-shell excitation yields depend on the depth penetrated into the target. To lowest order, this depth dependence may be described by means of a simple relation for the equivalent photon pulse responsible for the distant collision contribution. In the comprehensive treatment, the target response is examined in detail, *a priori* splitting between real and virtual photons is avoided, and influence of actual target geometry (tilt and finite thickness) is considered. Upon inclusion of a relatively small intensity component, the simple relation produces K-shell excitation yields, which are accurate to the percent level at any sample thickness for target atomic numbers above ten. The theory developed explains all existing experimental data.

I. INTRODUCTION

In 1940, Fermi[1] demonstrated theoretically that the ionization energy loss experienced by a charged-particle penetrating matter saturates at ultrarelativistic impact energies. The saturation appears as a result of the reduction, due to target polarization, in the action radius of the electromagnetic field of the projectile inside the medium. Accordingly, it is known as the *density effect*. The energy-loss phenomena studied by Fermi which, by now, are well-established experimentally too[2] are directly connected to the excitation and ionization of the individual target electrons. In consequence, the strong influence of target polarization should also be found in measurements of cross sections for the latter processes. This fact was first pointed out by Dangerfield[3] in 1973.

Already three years earlier, Middleman *et al.*[4] had published detailed experimental measurements of K-shell excitation using 0.15–0.9-GeV electrons incident on a wide range of targets ($29 \leq Z \leq 83$). Rather than showing any sign of saturation, the recorded yields increased proportionally to the logarithm of the Lorentz factor γ, the projectile energy in units of its rest mass. With the appearance of Dangerfield's paper, the lack of the density effect mystery was established. In the following years many new electron experiments[5–9] were set up in order to resolve the apparent discrepancy with theory. Despite a larger range of impact energies and target materials, and inclusion also of L and M shells, no moderation in the increase of yields was recorded even at the highest energies (Fig. 1). This pattern was not broken until 1983, when the experiment reported in Ref. 10 revealed some, although not full, density effect in K-shell excitation in aluminum and copper foils (Fig. 1). A large γ variation was obtained by the use of a secondary 5 GeV/c beam for which the yields of characteristic x rays induced upon pion and positron impact were measured relative to the x-ray yield recorded for protons.

The apparent inconsistency between theory and empirical data, Fig. 1, led us to a reconsideration of the theoretical situation. Through this work we realized that many speculations brought up by other authors to explain the lack of the density effect should be discarded.[11–12] Further on, it became clear that full density effect is not reached until after some depth in the target and that, during the setting up of the polarization fields, *transition radiation* is emitted which acts as an x-ray source located in the surface region of the target. To account for such effects, we have developed a new theory. Even in its most primitive form it provides good agreement between measured and calculated yields for all cases considered.[12]

In the present paper a comprehensive account is given of the new theoretical model for K-shell excitations caused by ultrarelativistic charged projectiles. We adapt the Weizsäcker-Williams method of virtual photons[13–14] in our calculations as this allows, in a simple way, for a transparent discussion of the influence of target polarization. The method is often abandoned by specialists since it is less accurate at nonrelativistic impact. However, at the ultrarelativistic energies of interest in the present context, the accuracy is comparable to that of much more elaborate theories. The lowest-order version of our model for the depth dependence of the K-shell excitation yield was presented earlier.[11,12] It essentially boils down to a summation of the intensity $dI_0/d\omega$ of virtual photons traveling along with the projectile throughout an infinite polarizable medium and the intensity $dI^{\mathrm{TR}}/d\omega$

of transition-radiation photons which, being real, is depleted with increasing depth, z, penetrated into the target, i.e., the total photon intensity responsible for the distant collision contribution to the excitation yield is approximated by the expression

$$\frac{dI}{d\omega}=\frac{dI_0}{d\omega}+\frac{dI^{\mathrm{TR}}}{d\omega}e^{-z/\lambda_a(\omega)}, \tag{1}$$

where λ_a denotes the absorption length of photons of frequency ω. For $z=0$, $dI/d\omega$ reduces to the virtual photon spectrum $dI^V/d\omega$ applying for motion in vacuum,

$$\frac{dI^V}{d\omega}\simeq\frac{dI_0}{d\omega}+\frac{dI^{\mathrm{TR}}}{d\omega}. \tag{2}$$

This observation was crucial for the understanding of experimental data which mostly have been recorded for thin targets.[10–12] In the comprehensive theory, Sec. II, we avoid the dubious ingredients of the simple model, especially the *a priori* splitting between real and virtual photons and subsequent incoherent addition. Splitting seems doubtful inside the formation zone for transition radiation which is comparable in thickness to $\lambda_a(\omega)$ for low-Z materials. As a first step, general expressions, valid in any dielectric, are obtained for the various components of the total photon intensity. Then, for a medium responding like a free-electron gas it is shown how a relatively small interference term emerges in addition to the intensities included in Eq. (1). Thirdly, through the construction of a realistic model for the dielectric function, where an imaginary term accounts for absorption, correct depletion of the various intensity components is automatically assured. Further deviations from the free-electron gas results introduced by the adoption of a realistic target response are explored. As a fourth step, the influence of the actual target geometry is examined.

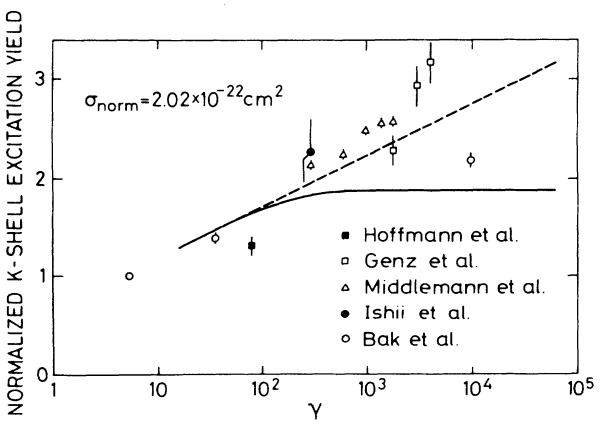

FIG. 1. K-shell excitation yield as a function of γ for projectiles of unit charge impinging on solid copper targets. The theoretical curves correspond to, respectively, inclusion (solid) and neglect (dashed) of the density effect. The experimental data are taken from Refs. 4, 6, 7, 9, and 10. The yields of Ref. 10 are displayed relative to that recorded for protons, the remaining data, and the curves are normalized to a cross section determined theoretically for 5 GeV/c protons (cf. Sec. III).

The main conclusion of the detailed analysis appears to be that, except for extremely low-Z materials, the simple model, as based on Eqs. (1) and (2), provides a fairly accurate first estimate of the inner-shell excitation yield at ultrarelativistic charged-particle impact. It should be emphasized, however, that through the comprehensive study deep insight is gained into the interplay and competition between the various polarization phenomena which determine the depth dependence of the excitation yield at high energies and, as a result, the very interpretation of experimental data is revised. We complete the discussion by comparing our results with experimental data and by quoting a few scaling relations (Secs. III and IV).

II. THEORY

In the semiclassical treatment Williams[13] groups collisions between the projectile and an atom into close and distant encounters. The cross section splits correspondingly,

$$\sigma=\sigma_c+\sigma_d . \tag{3}$$

The contribution due to distant collisions, σ_d, is computed by application of the method of virtual quanta.[13,14]

The basic idea of the Weizsäcker-Williams method of virtual photons is to replace the perturbing fields of a rapidly moving projectile by an equivalent pulse of radiation and, then, determine the interaction between projectile and target through known cross sections for photon interaction.[13,14] For our case σ_γ^K is relevant, the photoelectric cross section for K-shell excitation. As a result, σ_d is given as

$$\sigma_d=\int_{\omega_K}^{\infty}d\omega\,\frac{1}{\hbar\omega}\frac{dI}{d\omega}\sigma_\gamma^K(\omega), \tag{4}$$

where $\hbar\omega_K$ denotes the minimum excitation energy, i.e., the energy at which the K absorption edge appears. The intensity $dI/d\omega$ of virtual photons of frequency ω is defined by the Fourier component $\mathbf{E}(\omega)$ of the total electric field according to the relation[13,14]

$$\frac{dI}{d\omega}=c\int_d^{\infty}d\rho\,\rho\,|\,\mathbf{E}(\rho,\omega)\,|^2, \tag{5}$$

where ρ denotes the impact parameter relative to the struck atom. The minimum d, which divides between close and distant collisions, is of the order of atomic dimensions. As a result of the integration in Eq. (5), d appears underneath a large logarithm. Consequently, the exact choice is not important. Following Williams, we use $d=(\hbar/2m\omega_K)^{1/2}$, which essentially reflects the radius of the electronical orbit under consideration. Through $\mathbf{E}(\omega)$, the distant collision contribution reflects the polarization of the target.

In order to avoid *ab initio* splitting of photon intensity into real transition radiation and virtual photons, we shall use the full expression for the total electric field in Eq. (5). Let $\mathbf{E}_0$ represent the solution to the inhomogeneous Maxwell equations, which corresponds to the

charge and current density of a rapidly moving charged particle embedded in an infinite polarizable medium characterized by the dielectric function $\epsilon(\omega)$. In the penetration of the target surface it is necessary to fulfill the proper boundary conditions, namely, that the normal component of $\mathbf{B}$ and the tangential component of $\mathbf{E}$ be continuous. Hence, to obtain the total electric field, we add to the partial solution $\mathbf{E}_0$ a component $\mathbf{E}'$ which solves the homogeneous Maxwell equations in such a way that

$$\mathbf{E}_{\rm tot}\equiv\mathbf{E}_0+\mathbf{E}' \tag{6}$$

fulfills the boundary conditions. When the total electric field is determined for a given target geometry and dielectric function, we shall convert it to a photon intensity, i.e.,

$$\begin{aligned}\frac{dI}{d\omega}&=c\int^{\infty}d\rho\,\rho\,|\,\mathbf{E}_{\rm tot}(\rho,\omega)\,|^2\\&=c\int^{\infty}d\rho\,\rho[\,|\,\mathbf{E}_0\,|^2+|\,\mathbf{E}'\,|^2+2{\rm Re}(\mathbf{E}'\cdot\mathbf{E}_0^*)]\\&\equiv\frac{dI_0}{d\omega}+\frac{dI'}{d\omega}+\frac{dI^{\rm mix}}{d\omega}\ .\end{aligned} \tag{7}$$

As in Eq. (5), the lower limit of integration in the first term, $dI_0/d\omega$, is $\rho_{\rm min}=d$. For the last two terms we may choose $\rho_{\rm min}=0$, since E' falls off appreciably for distances smaller than the screening length in the electron gas, $c/\omega_p\sim10^2$ Å, and essentially has vanished at the very short distance $\rho\sim d\sim0.5$ Å$/Z$ (see below). Insertion of the intensity (7) into Eq. (4) yields σ_d.

In close collisions, the momentum transfer to the target electron attains values $\gtrsim\hbar/d$. This leads to an energy transfer in excess of the excitation energy, $w\gtrsim\hbar\omega_K$, with the choice $d=(\hbar/2m\omega_K)^{1/2}$. Hence the contribution σ_c essentially may be obtained from the differential cross section $d\sigma/dw$ for collisions between free particles as

$$\sigma_c=\int_{\hbar\omega_K}^{w_{\rm max}}dw\,\frac{d\sigma(w)}{dw}\ , \tag{8}$$

where the maximum energy transfer $w_{\rm max}$ is determined by the kinematics. Clearly, σ_c is independent of target polarization. It therefore appears as a z-independent background contribution whose magnitude is only of interest when comparisons are made with experimental data (Sec. III).

A. General expressions for photon intensities in semi-infinite target

In order to determine the total photon intensity, Eq. (7), inside a target consider first the component $dI_0/d\omega$. For a projectile of charge Z_pe and constant velocity $\mathbf{v}=\beta c\hat{\mathbf{z}}$ penetrating an infinite medium characterized by a frequency-dependent dielectric function $\epsilon(\omega)$, the total electromagnetic field as observed at the point $(z,x,y)=(0,\rho,0)$ is given by standard expressions[14]

$$\begin{aligned}E_z^0(\omega)&=-\frac{iZ_pe}{\omega}\left[\frac{2}{\pi}\right]^{1/2}\frac{\chi^2}{\epsilon(\omega)}K_0(\chi\rho)\ ,\\E_x^0(\omega)&=\frac{Z_pe}{v}\left[\frac{2}{\pi}\right]^{1/2}\frac{\chi}{\epsilon(\omega)}K_1(\chi\rho)\ ,\\B_y^0(\omega)&=\epsilon(\omega)\beta E_x^0(\omega)\ ,\\E_y^0&=B_x^0=B_z^0=0\ .\end{aligned} \tag{9}$$

Here K_n denotes a modified Bessel function of order n and the quantity χ is defined by the relation

$$\chi^2=\frac{\omega^2}{v^2}[1-\beta^2\epsilon(\omega)] \tag{10}$$

and chosen to lie in the fourth quadrant. At high values of $\gamma\equiv(1-\beta^2)^{-1/2}$, the field is similar to that of a pulse of electromagnetic radiation which justifies the Weizsäcker-Williams construction, Eqs. (4) and (5), cf. Refs. 14 and 15. Since the field $\mathbf{E}_0$, Eq. (9), as well as $\mathbf{E}'$ is linear in the projectile charge, all photon intensities scale as Z_p^2. For convenience in writing we drop such factors below and consider unit projectile charge. By means of Eqs. (9) and (5) we then obtain

$$\frac{dI_0}{d\omega}=-\frac{2}{\pi}\alpha\hbar\frac{d}{\beta^2{\rm Im}\epsilon}{\rm Im}\left[K_1(\bar{\chi}d)K_0(\chi d)\frac{\bar{\chi}(1-\beta^2\epsilon)}{\epsilon}\right]\ , \tag{11}$$

where $\alpha=e^2/\hbar c$ denotes the fine-structure constant. The notation $\bar{z}$ is used for the complex conjugate of z.

Let us next turn to the intensity components $dI'/d\omega$ and $dI^{\rm mix}/d\omega$ [Eq. (7)]. For a projectile incident along the surface normal (z axis) on a thick (i.e., semi-infinite) target characterized by a dielectric function $\epsilon(\omega)$, the correction $\mathbf{E}'$ to the asymptotic field $\mathbf{E}_0$ attains the value

$$\mathbf{E}'(\mathbf{r},t)=\int\mathbf{E}'(\mathbf{k})e^{i(\boldsymbol{\kappa}\cdot\boldsymbol{\rho}+\lambda z-\omega t)}d\mathbf{k},\quad\omega=k_zv \tag{12}$$

according to Garibian[16] (see also Ref. 17). The quantities $\boldsymbol{\kappa}$ and $\boldsymbol{\rho}$ denote the transverse components of $\mathbf{k}$ and $\mathbf{r}$, respectively, and $\mathbf{E}'(\mathbf{k})$ is given as

$$\mathbf{E}'_{\perp}(\boldsymbol{\kappa})=\frac{ei}{2\pi^2}\frac{\boldsymbol{\kappa}\lambda}{\zeta}\eta,\quad E'_{\parallel}(\mathbf{k})=-\frac{ei}{2\pi^2}\frac{\kappa^2}{\zeta}\eta\ , \tag{13}$$

with the definitions

$$\begin{aligned}\eta&=\frac{\epsilon^{-1}-\frac{v}{\omega}\lambda_0}{k^2-\frac{\omega^2}{c^2}\epsilon}+\frac{-1+\frac{v}{\omega}\lambda_0}{k^2-\frac{\omega^2}{c^2}}\ ,\\\zeta&=\lambda-\lambda_0\epsilon\ ,\\\lambda_0^2&=\left[\frac{\omega}{c}\right]^2-k^2\ ,\\\lambda^2&=\epsilon\left[\frac{\omega}{c}\right]^2-k^2\ ,\end{aligned} \tag{14}$$

where λ_0 and λ are chosen in the third and first qua-

drant, respectively. The transform $\mathbf{E}'(\mathbf{r},\omega)$ is obtained as

$$\mathbf{E}'(\mathbf{r},\omega)=\sqrt{2\pi}\int \mathbf{E}'(\mathbf{k})e^{i(\kappa\rho\cos\phi+\lambda z)}\kappa\, d\kappa\, d\phi/v \ , \tag{15}$$

where ϕ denotes the angle between $\boldsymbol{\kappa}$ and $\boldsymbol{\rho}$. The front factor $\sqrt{2\pi}$ is included to follow our previous convention for Fourier transforms. With the identity[18]

$$\int_0^{2\pi} e^{iz\cos\phi}\cos(n\phi)d\phi=2\pi i^n J_n(z) \ , \tag{16}$$

we may write Eq. (15) in terms of Bessel functions as

$$\begin{aligned} E'_\perp(\mathbf{r},\omega)&=-\frac{e}{v}\left[\frac{2}{\pi}\right]^{1/2}\int_0^\infty d\kappa\,\kappa^2 e^{i\lambda z}J_1(\kappa\rho)\frac{\lambda\eta}{\zeta} \ , \\ E'_\parallel(\mathbf{r},\omega)&=-i\frac{e}{v}\left[\frac{2}{\pi}\right]^{1/2}\int_0^\infty d\kappa\,\kappa^3 e^{i\lambda z}J_0(\kappa\rho)\frac{\eta}{\zeta} \ , \end{aligned} \tag{17}$$

where $\mathbf{E}'_\perp\|\boldsymbol{\rho}$.

Let us determine the photon intensity $dI'/d\omega$, Eq. (7), corresponding to $|\mathbf{E}'|^2$. With the relation[14]

$$\int_0^\infty d\rho\,\rho J_n(\kappa'\rho)J_n(\kappa\rho)=\frac{1}{\kappa}\delta(\kappa-\kappa') \ , \tag{18}$$

we get for the intensity belonging to the transverse component $E'_\perp$ the expression

$$\begin{aligned} \frac{dI'_\perp}{d\omega}&\equiv c\int_0^\infty d\rho\,\rho\,|E'_\perp|^2 \\ &=\frac{2}{\pi}\frac{e^2c}{v^2}\int_0^\infty d\kappa\int_0^\infty d\kappa'\kappa^2\kappa'^2 e^{-i\bar{\lambda}(\kappa')z}e^{i\lambda(\kappa)z} \\ &\quad\times\frac{\bar{\lambda}(\kappa')\lambda(\kappa)\bar{\eta}(\kappa')\eta(\kappa)}{\bar{\zeta}(\kappa')\zeta(\kappa)}\frac{1}{\kappa} \\ &\quad\times\delta(\kappa-\kappa') \ . \end{aligned} \tag{19}$$

Hence

$$\frac{dI'_\perp}{d\omega}=\frac{2}{\pi}\alpha\hbar\beta^{-2}\int_0^\infty d\kappa\,\kappa^3 e^{i(\lambda-\bar{\lambda})z}\frac{|\lambda|^2|\eta|^2}{|\zeta|^2} \ . \tag{20}$$

Similarly, the result for the intensity belonging to $E'_\parallel$ is

$$\frac{dI'_\parallel}{d\omega}=\frac{2}{\pi}\alpha\hbar\beta^{-2}\int_0^\infty d\kappa\,\kappa^5 e^{i(\lambda-\bar{\lambda})z}\frac{|\eta|^2}{|\zeta|^2} \ . \tag{21}$$

Among the mixed terms which correspond to $2\mathrm{Re}(\mathbf{E}'\cdot\mathbf{E}_0^*)$, consider first $dI_\perp^{\mathrm{mix}}/d\omega$. For $\mathbf{E}^0$, Eq. (9) applies except than an extra phase $e^{iz\omega/v}$ must be included to account for the observation point being moved from $(0,\rho,0)$ to $(z,\rho,0)$. Hence we have

$$E_\perp^0=\frac{e}{v}\left[\frac{2}{\pi}\right]^{1/2}\frac{\chi}{\epsilon}K_1(\chi\rho)e^{iz\omega/v} \ , \tag{22}$$

where χ, defined by Eq. (10), lies in the fourth quadrant. The ρ integration may be performed by virtue of the identity[19]

$$\int_0^\infty d\rho\,\rho J_n(\kappa\rho)K_n(\chi\rho)=\frac{\kappa^n}{\chi^n(\chi^2+\kappa^2)}, \quad n\geq 0 \tag{23}$$

and we obtain

$$\frac{dI_\perp^{\mathrm{mix}}}{d\omega}=-\frac{4}{\pi}\alpha\hbar\frac{1}{\beta^2}\mathrm{Re}\left[\int_0^\infty d\kappa\,\frac{\kappa^3}{\kappa^2+\chi^2}\frac{\lambda\eta}{\zeta\bar{\epsilon}}e^{i\lambda z-iz\omega/v}\right] . \tag{24}$$

Similarly, the result for the photon intensity belonging to the longitudinal field component is

$$\begin{aligned} \frac{dI_\parallel^{\mathrm{mix}}}{d\omega}&=-\frac{4}{\pi}\alpha\hbar\frac{1}{\beta^2}\frac{v}{\omega} \\ &\quad\times\mathrm{Re}\left[\int_0^\infty d\kappa\,\frac{\kappa^3}{\kappa^2+\chi^2}\frac{\eta\bar{\chi}^2}{\zeta\bar{\epsilon}}e^{i\lambda z-iz\omega/v}\right] . \end{aligned} \tag{25}$$

The sum of the expressions (11), (20), (21), (24), and (25) defines the total photon intensity. In the present form, the result is valid in general for any dielectric.

B. Application to free-electron gas

In the determination of the distant collision contribution to the K-shell excitation cross section according to Eq. (4), only frequencies above the K edge enter. In this region, which essentially is beyond all atomic resonances, we expect the screening electrons to respond, to a good approximation, as a free-electron gas. Hence for the dielectric function we substitute the expression

$$\epsilon(\omega)=1-\omega_p^2/\omega^2, \quad \omega_p^2=4\pi ne^2/m \ , \tag{26}$$

where ω_p denotes the plasma frequency of the gas of density n.

In order to obtain simple analytical expressions for the various photon intensities entering Eq. (7), a few additional approximations are applied. Firstly, since $\omega\geq\omega_K$, we have

$$1-\epsilon=\left[\frac{\omega_p}{\omega}\right]^2\leq\left[\frac{\omega_p}{\omega_K}\right]^2\ll 1 \ . \tag{27}$$

For e.g., copper, the latter ratio is smaller than 10^{-4}. In front factors in equations such as (24)–(25), it is therefore adequate to put $\epsilon=1$. Secondly, in discussing the density effect, we consider $\gamma\gtrsim 10^2$, cf. Fig. 1, corresponding to $1-\beta^2\lesssim 10^{-4}$. It is therefore also adequate to put $\beta=1$ in front factors as well as replace $\beta\gamma$ underneath logarithms simply by γ. Finally, we shall apply a long-distance approximation in the expressions for $dI'/d\omega$, $dI^{\mathrm{mix}}/d\omega$. Since the adjustment of the projectile field at high γ values takes place at distances $\rho\gtrsim c/\omega_p$ (see below), we have $\kappa^{-1}\sim\rho\gtrsim c/\omega_p$, and thereby

$$\frac{c\kappa}{\omega}\lesssim\frac{\omega_p}{\omega}<\frac{\omega_p}{\omega_K}\ll 1 \ . \tag{28}$$

With the response function (26) of a free-electron gas, $\mathrm{Im}\epsilon$ is infinitesimal and $\epsilon_r=\mathrm{Re}\epsilon$ is less than 1. We therefore expand the expression (11) to yield

$$\frac{dI_0}{d\omega}=\frac{2}{\pi}\alpha\hbar\frac{1}{\beta^2|\epsilon|^2}\left[\xi K_0(\xi)K_1(\xi)-\frac{\epsilon_r\beta^2}{2}[K_1^2(\xi)-K_0^2(\xi)]\xi^2\right], \tag{29}$$

$$\xi\equiv\frac{d\omega}{v}\sqrt{1-\epsilon_r\beta^2}\ .$$

For $\omega\sim\omega_K$ and $v\sim c$, we have $d\omega/v\ll 1$. Consequently, in view of the inequality (27), and with β close to 1, the quantity ξ is small. Expansion of Eq. (29) leads, with $\epsilon_r=\epsilon$ given by Eq. (26), to the result

$$\frac{dI_0}{d\omega}=\frac{2}{\pi}\alpha\hbar\left[\ln\left\{\frac{1.123c\gamma}{d\omega}\left[1+\left[\frac{\gamma\omega_p}{\omega}\right]^2\right]^{-1/2}\right\}-\frac{1}{2}\right]$$

$$=\frac{2}{\pi}\alpha\hbar\left[\ln\left[\frac{1.123\rho_{\max}}{d}\right]-\frac{1}{2}\right]. \tag{30}$$

In Eq. (30), factors of ϵ and β have been set identical to 1 as described above [i.e., where explicit in Eq. (29) except in the expression for ξ]. According to Eq. (9), the range of fields is $\sim\rho_{\max}\equiv\chi^{-1}$ since the modified Bessel functions K_n fall off exponentially for arguments larger than 1. As indicated by the last equality, the expression (30) is defined essentially by the logarithm of the ratio of this range to the dividing distance d.

For the special case of motion in vacuum, the virtual-photon spectrum (30) reduces to

$$\frac{dI^V}{d\omega}=\frac{2}{\pi}\alpha\hbar\left[\ln\left[\frac{1.123c\gamma}{d\omega}\right]-\frac{1}{2}\right], \tag{31}$$

corresponding to an effective maximum impact parameter of $\rho_{\max}^V=c\gamma/\omega$.

In case γ attains values lower than the critical measure

$$\gamma_c\equiv\omega/\omega_p\ , \tag{32}$$

which for, e.g., copper attains the value 154 at $\omega=\omega_K$, the virtual-photon spectrum, Eq. (30), is essentially unaffected by medium polarization, $\rho_{\max}\simeq\rho_{\max}^V$. The spectrum is defined by the vacuum value, Eq. (31), which increases with $\ln\gamma$. On the other hand, for $\gamma>\gamma_c$ the spectrum $dI_0/d\omega$ saturates into a γ-independent constant as the range of fields saturates towards the limit c/ω_p. This reduction, which is directly reflected to the excitation cross section, is the density effect. The limiting value reached at high impact energies is intimately connected to the Fermi plateau appearing in ionization energy loss. We note that with a typical value for ω_p in solids, $\hbar\omega_p\sim 20$ eV, the asymptotic range c/ω_p amounts to $\sim 10^2$ Å, i.e., it is considerably larger than the interatomic distance.

Let us now consider the contributions $dI'/d\omega$ and $dI^{\rm mix}/d\omega$. By virtue of Eq. (28), we obtain from Eq. (14) by insertion of the dielectric function (26) the expressions

$$\lambda_0=-\frac{\omega}{c}\left[1-\frac{1}{2}\left[\frac{\kappa c}{\omega}\right]^2\right],$$

$$\lambda=\frac{\omega}{c}\left[1-\frac{1}{2}\frac{\omega_p^2}{\omega^2}-\frac{1}{2}\left[\frac{\kappa c}{\omega}\right]^2\right], \tag{33}$$

$$\zeta=\frac{\omega}{c}\left[2-\frac{3}{2}\frac{\omega_p^2}{\omega^2}-\left[\frac{\kappa c}{\omega}\right]^2\right].$$

With $\epsilon=1=\beta$ in front factors and $\beta\gamma$ replaced by γ, we therefore get for the quantity $\lambda\eta/\zeta$ to be inserted in Eqs. (20) and (24), η being defined in Eq. (14), the result

$$\frac{\lambda\eta}{\zeta}=-\frac{\omega_p^2}{c^2}\left[\kappa^2+\left[\frac{\omega}{\gamma c}\right]^2+\frac{\omega_p^2}{c^2}\right]^{-1}\left[\kappa^2+\left[\frac{\omega}{\gamma c}\right]^2\right]^{-1}. \tag{34}$$

Similarly, η/ζ, to enter Eqs. (21) and (25), is given as

$$\frac{\eta}{\zeta}=-\frac{\omega_p^2}{c^2}\frac{c}{\omega}\left[\kappa^2+\left[\frac{\omega}{\gamma c}\right]^2+\frac{\omega_p^2}{c^2}\right]^{-1}\left[\kappa^2+\left[\frac{\omega}{\gamma c}\right]^2\right]^{-1}. \tag{35}$$

From these expressions it is evident that the photon intensities $dI'/d\omega$ and $dI^{\rm mix}/d\omega$, Eqs. (20), (21), (24), and (25), only receive contributions from κ values which fulfill the condition

$$\frac{c\kappa}{\omega}\lesssim\max(\gamma^{-1},\omega_p/\omega)\ll 1\ , \tag{28'}$$

in accordance with the approximation (28).

The conditions (27) and (28) assure that the quantity λ is real, $\lambda=\bar{\lambda}$. It is then a simple exercise to insert Eq. (34) into Eq. (20) and perform the κ integration. The result is that

$$\frac{dI_\perp'}{d\omega}=\frac{2}{\pi}\alpha\hbar\left\{\left[\frac{1}{2}+\left[\frac{\omega}{\gamma\omega_p}\right]^2\right]\ln\left[1+\left[\frac{\gamma\omega_p}{\omega}\right]^2\right]-1\right\}$$

$$=\frac{dI^{\rm TR}}{d\omega}\ , \tag{36}$$

i.e., the standard expression for the intensity of transition radiation[14] is obtained for $dI_\perp'/d\omega$. By comparison to Eqs. (30) and (31), the approximate relation (2) is easily verified. For $\gamma<\gamma_c$, the transition radiation spectrum falls off very rapidly since essentially no field adjustment takes place. For $\gamma>\gamma_c$, a substantial burst of radiation is emitted. The correlation to the appearance of the density effect is clearly displayed if the transition radiation spectrum is expressed in terms of maximal impact parameters,

$$\frac{dI^{\rm TR}}{d\omega}=\frac{2}{\pi}\alpha\hbar\left[\left[1+\frac{2}{(\rho_{\max}^V/\rho_{\max})^2-1}\right]\times\ln\left[\frac{\rho_{\max}^V}{\rho_{\max}}\right]-1\right]. \tag{36'}$$

We emphasize that the result (36) holds at all depths z, especially also inside the radiation formation zone, $0<z<l$. From Eqs. (34), (35), (20), and (21) it is further apparent that

$$\frac{dI'_{\parallel}}{d\omega}\Big/\frac{dI'_{\perp}}{d\omega}=\left[\frac{\kappa c}{\omega}\right]^2 . \tag{37}$$

The ratio should be understood as the ratio before the final κ integration. By virtue of Eq. (28), the contribution $dI'_{\parallel}/d\omega$ is totally negligible.

For the ratio of the mixed intensities a relation similar to Eq. (37) holds, namely,

$$\frac{dI_{\parallel}^{\mathrm{mix}}}{d\omega}\Big/\frac{dI_{\perp}^{\mathrm{mix}}}{d\omega}\simeq\left[\frac{\chi c}{\omega}\right]^2<\left[\frac{\omega_p}{\omega}\right]^2 . \tag{38}$$

We therefore again concentrate on the transverse contribution. This may be rewritten as

$$\frac{dI_{\perp}^{\mathrm{mix}}}{d\omega}=\frac{4}{\pi}\alpha\hbar\frac{\omega_p^2}{c^2}\mathrm{Re}\left\{\int_0^{\infty}d\kappa\,\kappa^3 e^{i[(\omega/v)-\lambda]z}\times\left[\kappa^2+\left[\frac{\omega}{\gamma c}\right]^2+\left[\frac{\omega_p}{c}\right]^2\right]^{-2}\times\left[\kappa^2+\left[\frac{\omega}{\gamma c}\right]^2\right]^{-1}\right\}, \tag{39}$$

where the phase in the exponential may be expressed as

$$\left[\frac{\omega}{v}-\lambda\right]z\simeq\frac{\omega z}{2c}\left[\gamma^{-2}+\frac{\omega_p^2}{\omega^2}+\left[\frac{\kappa c}{\omega}\right]^2\right]=\frac{z}{l(\omega)}+\frac{\omega z}{2c}\left[\frac{\kappa c}{\omega}\right]^2 . \tag{40}$$

The formation length $l(\omega)$ is defined as

$$l(\omega)=\frac{2\gamma_c c/\omega_p}{1+(\gamma_c/\gamma)^2} . \tag{41}$$

By a change of variable we write Eq. (39) as

$$\frac{dI_{\perp}^{\mathrm{mix}}}{d\omega}=\frac{1}{\pi}\alpha\hbar\frac{z\omega_p^2}{\omega c}\int_{z/l}^{\infty}dt\,\cos t\left[\frac{1}{t^2}-\frac{z\omega/2\gamma^2 c}{t^2(t-\xi z)}\right], \qquad \xi\equiv\frac{\omega_p^2}{2\omega c}=\frac{l^{-1}}{1+\gamma_c^2/\gamma^2} . \tag{42}$$

After the second term has been split into partial fractions, we may perform the t integration with the result that

$$\frac{dI_{\perp}^{\mathrm{mix}}}{d\omega}=\frac{2}{\pi}\alpha\hbar\left[\cos(z/l)+\frac{z}{l}\mathrm{si}(z/l)-\frac{\gamma_c^2}{\gamma^2}[\sin(\xi z)\mathrm{si}(\xi' z)-\cos(\xi z)\mathrm{Ci}(\xi' z)+\mathrm{Ci}(z/l)]\right],$$

$$\xi'\equiv\frac{l^{-1}}{1+\gamma^2/\gamma_c^2}=\frac{\gamma_c^2}{\gamma^2}\xi , \tag{43}$$

where si,Ci denote the sine, cosine integral.[18,19]

Let us evaluate the general expression (43) in various limits. For $z=0$ a small argument expansion of the si and Ci functions leads to the result

$$\frac{dI_{\perp}^{\mathrm{mix}}}{d\omega}(z=0)=\frac{2}{\pi}\alpha\hbar\left[1-\frac{\gamma_c^2}{\gamma^2}\ln\left[1+\frac{\gamma^2}{\gamma_c^2}\right]\right] \tag{44}$$

and in turn, by comparing to Eqs. (36), (30), and (31), to the exact relation

$$\frac{dI_0}{d\omega}+\frac{dI'}{d\omega}+\frac{dI^{\mathrm{mix}}}{d\omega}\bigg|_{z=0}=\frac{dI^V}{d\omega} . \tag{45}$$

Hence continuity is maintained at the target surface, where the intensity $dI^{\mathrm{mix}}/d\omega$ accounts for the term missing in the simple model, [cf. Eq. (2)].

The dependence on penetrated depth of the mixed photon intensity, Eq. (43), is illustrated in Fig. 2 for various values of the parameter γ/γ_c. The intensity is largest for $\gamma\gg\gamma_c$ where the density effect also appears. Here Eq. (43) reduces by neglect of the last term in large parentheses to

$$\frac{dI_{\perp}^{\mathrm{mix}}}{d\omega}=\frac{2}{\pi}\alpha\hbar\left[\cos(z/l)+\frac{z}{l}\mathrm{si}(z/l)\right],\quad \gamma\gg\gamma_c . \tag{46}$$

The amplitude of the oscillating function in Eq. (46) is damped with increasing depth z so that the function attains its maximum at $z=0$, namely 1, whereas for $l<z$ it decreases as $-(l/z)\sin(z/l)$ (cf. Ref. 18). [For $z>l\gamma^2/\gamma_c^2$, where it is no longer permissible to neglect the last term in Eq. (43), an even more rapid decrease is encountered.] Hence the contribution due to the mixed term is always small, never exceeding the formation zone maximum of $2\alpha\hbar/\pi$ which corresponds to, typically, 10% of the total photon intensity. In the opposite extreme, $\gamma\ll\gamma_c$, the intensity $dI^{\mathrm{mix}}/d\omega$ essentially vanishes. Indeed, already for $\gamma/\gamma_c=0.5$ the quantity in large parentheses is smaller than ~ 0.1 at all depths (cf. Fig. 2).

It is now clear that if we neglect the small mixed intensity, we retrieve our previous simple ansatz (1), for the moment without the exponential since absorption has been ignored. It should be emphasized again that the relation holds at all z, especially also inside the for-

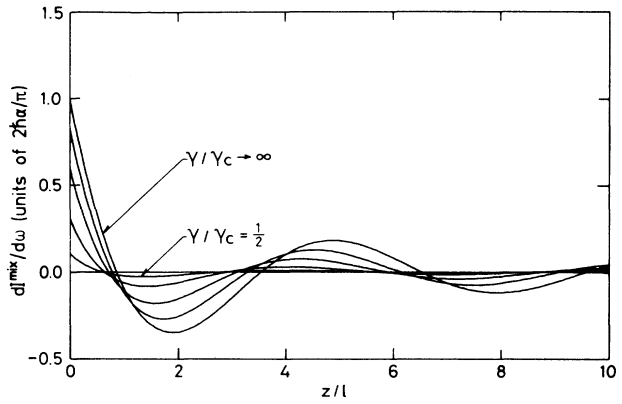

FIG. 2. The mixed intensity, Eq. (43), as a function of penetrated depth for $\gamma/\gamma_c = 1/2$, 1, 2, 4, and $\gamma/\gamma_c \to \infty$. The quantity l denotes the formation length. Note that absorption is neglected.

mation zone $z < l$. On the other hand, it is also obvious that for $z < l$ we can no longer interpret the two terms separately as belonging to the projectile field and real TR photons, respectively. The separation process is inherent in the appearance of $dI^{\rm mix}/d\omega$. This interference term survives as long as the shaking off of real photons takes place. For $z > l$ the process of creation of real TR photons is essentially finished, and $dI^{\rm mix}/d\omega$ drops off (cf. Fig. 2). It should be stressed that the physical reason for the lack of the density effect in experiments where the target thickness attains values of $t < l$ $[< \lambda_a(\omega)]$ is that such targets are too thin for a field adjustment to develop. As a result the virtual-photon intensity inside the foil remains essentially unchanged with respect to its vacuum value and no transition radiation is emitted. Also in this case Eq. (1) therefore remains valid but the full intensity should be interpreted as belonging to virtual photons.

C. Photon intensities for realistic dielectric function

In Sec. II B we considered a target responding as a nonabsorbing free-electron gas. Let us now construct a more realistic expression for the target dielectric function, valid for frequencies above the K edge, and compute the corresponding changes introduced in the various photon intensities.

To account properly for absorption in the target medium, a positive imaginary term is included in the dielectric function which we express as

$$\epsilon = \epsilon_r + i\epsilon_i \equiv 1 - \frac{\tilde{\omega}_p^2}{\omega^2} + i\epsilon_i \ . \tag{47}$$

In general the quantity $\tilde{\omega}_p^2$ entering the real part ϵ_r of ϵ depends on frequency. From the dispersion relation $k = \sqrt{\epsilon}\omega/c$, where k denotes the wave number for a photon of frequency ω, it follows that ϵ_r and ϵ_i are connected to the real and imaginary parts of k, $k_r \equiv {\rm Re}k$, and $(2\lambda_a)^{-1} = {\rm Im}k$ through the relations

$$\begin{aligned} k_r^2 - 1/4\lambda_a^2 &= \omega^2\epsilon_r/c^2 \ , \\ k_r/\lambda_a &= \omega^2\epsilon_i/c^2 \ . \end{aligned} \tag{48}$$

The absorption length $\lambda_a(\omega)$ is determined by the total photoelectric cross section $\sigma_\gamma^{\rm tot}(\omega)$ as $\lambda_a^{-1} = n_a\sigma_\gamma^{\rm tot}$ with $n_a = n/Z$ denoting the density of target atoms. As we consider K-shell excitations, the frequency ω is never smaller than ω_K, which typically corresponds to an energy of a few keV. Consequently, k_r is of order 1 Å^{-1}. On the other hand, the absorption length attains values of the order of 1 μm, i.e., $\lambda_a^{-1} \sim 10^{-4}$ Å^{-1}. It is therefore completely safe to neglect λ_a in the first of Eq. (48). As a result we get

$$\epsilon_i = \sqrt{\epsilon_r}\frac{c}{\omega}\lambda_a^{-1}(\omega) = \frac{c}{\omega}\lambda_a^{-1}(\omega) \ . \tag{49}$$

Here the last equality holds since ϵ_r generally remains very close to 1 above the K edge, as we shall discuss below. It may be noted that $\epsilon_i/\epsilon_r = (k\lambda_a)^{-1} \sim 10^{-4}$.

The real part of the dielectric function may be obtained by use of the Kramers-Kronig relation[14]

$$\epsilon_r = 1 + \omega_p^2 \, {\rm P} \int_0^\infty d\omega' \frac{f(\omega')}{\omega'^2 - \omega^2} \ , \tag{50}$$

where P denotes the principal value. The generalized atomic oscillator strength $f(\omega)$ relates to the imaginary part ϵ_i as

$$\epsilon_i = \frac{\pi}{2}\frac{\omega_p^2}{\omega} f(\omega), \quad \int_0^\infty d\omega \, f(\omega) = 1 \ . \tag{51}$$

In view of Eq. (49) it is further proportional to the photoelectric cross section $f = 2cn_a\sigma_\gamma^{\rm tot}/\pi\omega_p^2$. If we assume $\sigma_\gamma^{\rm tot} \propto \omega^{-3}$, which scaling applies fairly well for many target materials above the K edge, cf. Refs. 20 and 21, Eq. (50) reduces, with the definition (47), to

$$\begin{aligned} \frac{\tilde{\omega}_p^2(\omega > \omega_K)}{\omega_p^2} &= \omega^2 \int_0^{\omega_K} d\omega' \frac{f(\omega')}{\omega^2 - \omega'^2} \\ &+ \left[1 + \frac{\omega_K^2}{\omega^2} \ln\left[\frac{\omega^2}{\omega_K^2} - 1 \right] \right] \int_{\omega_K}^\infty d\omega' f(\omega') \ . \end{aligned} \tag{52}$$

Since the oscillator strength decreases rapidly with increasing photon energy between the well-separated L and K edges, we shall neglect ω'^2 in the denominator in the first term and Eq. (52) simplifies to

$$\frac{\tilde{\omega}_p^2}{\omega_p^2} \simeq 1 + \frac{\omega_K^2}{\omega^2} \ln\left[\frac{\omega^2}{\omega_K^2} - 1 \right] \int_{\omega_K}^\infty d\omega' f(\omega') \ . \tag{53}$$

The integral in Eq. (53) attains values $\lesssim 2/Z$, the relative number of K electrons. For instance, in copper the oscillator strength, which remains above ω_K, amounts to $1.3/Z$. It is then clear that the quantity $\tilde{\omega}_p^2$ is close to the square of the plasma frequency, ω_p^2, except near the K edge. In this region, which is extremely narrow for targets of not very low-atomic numbers, ϵ_r may turn

larger than 1 cf. Eq. (78), and emission of Cherenkov radiation is allowed for. A simple analysis shows that such an emission leads to corrections in the total K-shell excitation yield of less than 1% as soon as $Z \gtrsim 10$. In the following it is therefore assumed that the real part of the dielectric function is less than 1, $0 < 1-\epsilon_r \ll 1$, and, in consequence, that $|1-\epsilon| \ll 1$.

Let us now turn to the photon spectra. The general expression for $dI_0/d\omega$ corresponding to an infinite medium is given in Eq. (11). With the above dielectric function and $|1-\beta| \ll 1$, the inequality $|1-\beta^2\epsilon| \ll 1$ is fulfilled. Since also $\omega d/c$ is small compared to 1 for $d \sim a_0/Z$ and frequencies of the order of ω_K ($\omega_K d/c \sim \alpha Z$), it is again a very good approximation indeed to perform a small argument expansion of the Bessel functions in Eq. (11). As usual, powers of β will be dropped in front factors and as a result we obtain

$$\frac{dI_0}{d\omega} = -\frac{2}{\pi}\alpha\hbar\frac{1}{\epsilon_i}\mathrm{Im}\left[\ln\left[\frac{1.123}{\chi d}\right]\frac{1-\beta^2\epsilon}{\epsilon}\right] . \tag{54}$$

It is safe also to put $|\epsilon|^2=1$ in the front factor and with $\chi = |\chi| e^{i\theta}$ Eq. (54) may be rewritten as

$$\frac{dI_0}{d\omega} = \frac{2}{\pi}\alpha\hbar\left[\ln\left[\frac{1.123}{|\chi| d}\right] + \frac{\epsilon_r - \beta^2|\epsilon|^2}{\epsilon_i}\theta\right] . \tag{55}$$

Here

$$\begin{aligned} |\chi| &= \frac{\omega}{\gamma c}[(1+\nu^{-2})^2+(\gamma^2\epsilon_i)^2]^{1/4} , \\ \theta &= -\frac{1}{2}\tan^{-1}\left[\frac{\gamma^2\epsilon_i}{1+\nu^{-2}}\right], \quad \nu \equiv \omega/\gamma\tilde{\omega}_p , \end{aligned} \tag{56}$$

since χ lies in the fourth quadrant, and as a final expression we get

$$\frac{dI_0}{d\omega} = \frac{2}{\pi}\alpha\hbar\left\{\ln\left[\frac{1.123\gamma c}{\omega d}[(1+\nu^{-2})^2+(R\nu^{-2})^2]^{-1/4}\right] - \frac{1+\nu^2}{2R}\tan^{-1}\left[\frac{R}{1+\nu^2}\right]\right\} . \tag{57}$$

A term of order $\epsilon_i (\ll 1)$ has been neglected compared with the logarithm which attains values of 5–10 at high γ. The quantity R is defined as

$$R \equiv \frac{\epsilon_i}{1-\epsilon_r} = \omega^2\epsilon_i/\tilde{\omega}_p^2 . \tag{58}$$

It may be noted that for $\epsilon_i = 0$, Eq. (57) reduces to the expression (30).

Due to the inclusion of finite ϵ_i, the γ value around which the density effect sets in is changed from expression (32) to the general critical value

$$\gamma_c = \frac{\omega}{\tilde{\omega}_p}(1+R^2)^{-1/4} . \tag{59}$$

This result indicates that as long as R is small we shall only expect minor corrections to the simple formulas Eqs. (1) and (2), where now ω_p is replaced with $\tilde{\omega}_p$. However, the density effect is also encountered in the extreme situation where $\tilde{\omega}_p^2 \to 0$. Here the spectrum (57) reduces to

$$\frac{dI_0}{d\omega} = \frac{2}{\pi}\alpha\hbar\left[\ln\left[\frac{1.123\gamma c}{\omega d}[1+(\gamma^2\epsilon_i)^2]^{-1/4}\right] - \frac{1}{2\gamma^2\epsilon_i}\tan^{-1}(\gamma^2\epsilon_i)\right] \tag{60}$$

with a critical γ value of $\gamma_c = \epsilon_i^{-1/2}$.

In order to apply the general expressions for the photon intensities $dI'/d\omega$ and $dI^{\mathrm{mix}}/d\omega$, Sec. II A, to a medium characterized by the dielectric function (47), we shall proceed as in Sec. II B. In analogy to Eq. (33), we then have

$$\begin{aligned} \lambda &= \frac{\omega}{c}\left[1-\frac{1}{2}\frac{\tilde{\omega}_p^2}{\omega^2}-\frac{1}{2}\left[\frac{\kappa c}{\omega}\right]^2+\frac{1}{2}i\epsilon_i\right] , \\ \zeta &= \frac{\omega}{c}\left[2-\frac{3}{2}\frac{\tilde{\omega}_p^2}{\omega^2}-\left[\frac{\kappa c}{\omega}\right]^2+\frac{3}{2}i\epsilon_i\right] , \end{aligned} \tag{61}$$

the expression for λ_0 given in Eq. (33) being unchanged. As an immediate consequence of the relation for λ, the exponential in the integrand in Eqs. (20) and (21) leads to depletion of $dI'/d\omega$ with penetrated depth,

$$\frac{dI'}{d\omega} \propto e^{i(\lambda-\bar{\lambda})z} = e^{-z/\lambda_a(\omega)} . \tag{62}$$

This is in agreement with our previous considerations which led to the simple formula (1). As to the mixed terms we get from the exponential in Eqs. (24) and (25), besides the phase given by the right-hand side of Eq. (40) with $\omega_p \to \tilde{\omega}_p$, a damping

$$\frac{dI^{\mathrm{mix}}}{d\omega} \propto e^{-z/2\lambda_a(\omega)} . \tag{63}$$

It should be emphasized that Eqs. (62) and (63) hold at all depths, especially also inside the formation zone. This fact, which might seem somewhat surprising since the individual photon intensities have no simple interpretation for $z \lesssim l$, justifies the way damping appears in the simple formula (1).

In order to evaluate the remaining changes introduced on the photon intensities $dI'/d\omega$ and $dI^{\mathrm{mix}}/d\omega$ with respect to the expressions given in Sec. II B, consider first the major component $dI'_\perp/d\omega$ [Eq. (20)]. Use of the approximations (27) and (28) leads to the relation

$$\frac{|\lambda|^2|\eta|^2}{|\zeta|^2} = \frac{1}{r}+\frac{1}{y^2}-\frac{2y_1}{ry}, \quad y=\kappa^2+(\omega/\gamma c)^2, \quad y_1 = y+\tilde{\omega}_p^2/c^2, \quad r = y_1^2+\omega^4\epsilon_i^2/c^4 . \tag{64}$$

By insertion of Eq. (64), the κ integration in Eq. (20) may be performed to yield the intensity

$$\frac{dI'_\perp}{d\omega}=\frac{2}{\pi}\alpha\hbar e^{-z/\lambda_a}\frac{1}{2}\left[\left[\frac{1}{2}+\frac{\nu^2}{1+R^2}\right]\ln[(1+\nu^{-2})^2+(R\nu^{-2})^2]-1+R^{-1}\left[\nu^2\frac{R^2-1}{R^2+1}-1\right]\tan^{-1}\left[\frac{R}{1+\nu^2}\right]\right], \quad (65)$$

which for $\epsilon_i\to 0$ reduces to $dI^{\mathrm{TR}}/d\omega$, Eq. (36), times the exponential damping.

The formula for the mixed intensity $dI_\perp^{\mathrm{mix}}/d\omega$, Eq. (24), may be rewritten as

$$\frac{dI_\perp^{\mathrm{mix}}}{d\omega}=-\frac{4}{\pi}\alpha\hbar e^{-z/2\lambda_a}\mathrm{Re}\left[\int_0^\infty d\kappa\,\kappa^3\left[\frac{1}{r}-\frac{1}{yy_2}\right]e^{-i(cz/2\omega)y_1}\right],$$

$$y_2=y_1+i\omega^2\epsilon_i/c^2\,, \quad (66)$$

with the notation introduced in Eq. (64). We have put $\bar{\epsilon}=1$ in the integrand. As noted above, the phase factor remaining underneath the integral is the same as in Eqs. (39) and (40), except for the substitution $\omega_p\to\tilde{\omega}_p$. Hence the formation length $l(\omega)$ remains unchanged by introduction of a finite ϵ_i as does its physical interpretation. For convenience we shall therefore only consider the simple case $z=0$. Here it is straightforward to perform the κ integration

$$\frac{dI_\perp^{\mathrm{mix}}}{d\omega}(z=0)=\frac{2}{\pi}\alpha\hbar\left[\left[\frac{1+\nu^2}{R}-\frac{\nu^2 R}{1+R^2}\right]\tan^{-1}\left[\frac{R}{1+\nu^2}\right]-\frac{1}{2}\frac{\nu^2}{1+R^2}\ln[(1+\nu^{-2})^2+(R\nu^{-2})^2]\right]. \quad (67)$$

In the limit $\epsilon_i\to 0$, Eq. (67) reduces to the previous result (44). It may be noted that $dI^{\mathrm{mix}}(z=0)/d\omega$ always attains values of order 1 [in units of $(2/\pi)\alpha\hbar$] to be compared with total intensities of order ~ 10. In the extreme case, where $\tilde{\omega}_p^2\to 0$, the mixed intensity actually vanishes.

At the target surface, $z=0$, the total photon intensity obtained by adding the three spectra, Eqs. (57), (65), and (67), equals the vacuum value $dI^V/d\omega$ given by Eq. (31). Hence continuity at the target surface is maintained also in the general case, where the dielectric function is given as in Eq. (47). Besides providing the exponential damping, Eqs. (62) and (63), the introduction of a finite ϵ_i as well as the substitution $\omega_p^2\to\tilde{\omega}_p^2$ therefore leads merely to a redistribution of intensity among the various terms dI_0, dI', and dI^{mix}. In Fig. 3 are shown $dI_0/d\omega$ (full drawn), $d(I_0+I')/d\omega$ for $z=0$ (dotted) and the total photon intensity also for $z=0$ (dashed) as functions of $\gamma/\tilde{\gamma}_c$ for $R=0$ and a few relatively large R values, $\tilde{\gamma}_c\equiv\omega/\tilde{\omega}_p=\gamma\nu$. All intensities are given relative to the "Fermi level" obtained from Eq. (30) for $R=0$ in the limit $\gamma\to\infty$ with $\omega_p\to\tilde{\omega}_p$. The total intensity for $z=0$, being equal to the vacuum intensity, is independent of R and the mixed intensity is always small, attaining its maximum of $2\hbar\alpha/\pi$ for $R=0$. On other hand, with increasing R value, the density effect sets in at a still lower γ value and the level of the Fermi plateau is reduced correspondingly, cf. Eq. (59).

Except for very low-Z materials (see later), and apart from a narrow frequency range near ω_K, the quantity R actually attains only small values. For R, $|1-\tilde{\omega}_p^2/\omega_p^2|<1$, the changes introduced in the various photon intensities given above, upon replacement of the simple dielectric function (26) by the expression (47), are

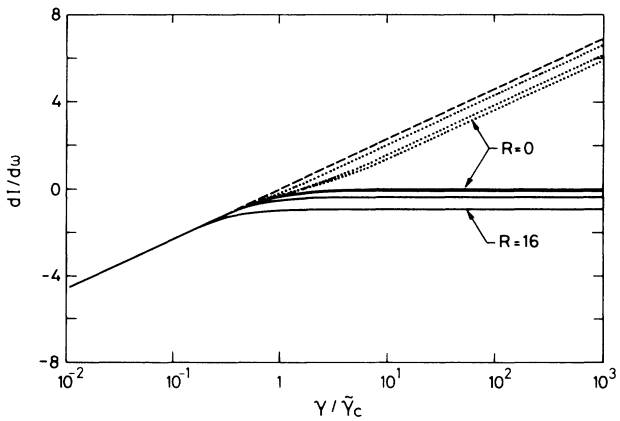

FIG. 3. The various photon intensities as a function of $\gamma/\tilde{\gamma}_c$ for $R=0,1,4,16$. The intensities are given in units of $2\hbar\alpha/\pi$ and relative to the Fermi plateau obtained for $R=0$. Solid curves correspond to $dI_0/d\omega$, Eq. (57), dotted curves to the sum of $dI_0/d\omega$ and $dI'/d\omega$ at the target surface, while the dashed curve represents the total intensity, for $z=0$, which equals the vacuum intensity. The solid curves for $R=0,1$ are hardly distinguishable whereas a dotted curve, corresponding to $R=16$, essentially would fall on the vacuum result.

in order of magnitude

$$\frac{2}{\pi}\hbar\alpha \max\left\{\left|1-\frac{\tilde{\omega}_p^2}{\omega_p^2}\right|, R^2\right\} . \tag{68}$$

Such corrections are clearly negligible. Also the changes in the total K-shell excitation yield deriving from the frequency range where R or $|1-\tilde{\omega}_p^2/\omega_p^2|$ attains values of the order of or larger than 1 are small for targets of not too low Z. As an example, even for aluminum overall changes in the excitation yield of less than 1% are encountered with respect to the results applying for a free-electron gas, Sec. II B, when exponential depletion, Eqs. (62) and (63), is included. We note that neither the Weizsäcker-Williams scheme applied here nor the experimental performance justifies discussion of such low effects. Nevertheless, we mention that, in any case, the changes in the total photon intensity are small near the target surface due to continuity.

D. Influence of target geometry

All considerations so far have been based on the assumption of a semi-infinite target and of incidence at right angle to the target surface. Clearly, in the experimental situation none of these conditions hold in general and we shall therefore evaluate the changes introduced in case of oblique incidence on a target of finite thickness.

As to the importance of non-normal incidence, it suffices to refer to the existing standard literature on transition radiation. As discussed by, e.g., Artru *et al.*[22] and Garibian[23] the transition-radiation spectrum is independent of the incidence angle as long as the radiation cone is completely contained inside the second medium, i.e., inside the target upon entrance and inside the vacuum on the back upon exit. As the opening angle θ of the radiation cone for a target described by the simple dielectric function, Eq. (26), is of order[22,23]

$$\theta \sim (\gamma^{-2}+\omega_p^2/\omega^2)^{1/2} , \tag{69}$$

which, in our case, is always small compared to 1, we may conclude that the formalism derived in Secs. II A–II C, in general, applies also to the case of oblique incidence. Indeed, since polarization effects are important only for $\gamma > \gamma_c \equiv \omega/\omega_p$, exclusively situations with grazing incidence at angles to the surface smaller than

$$\theta \sim \gamma_c^{-1} \leq \frac{\omega_p}{\omega_K} \tag{69'}$$

are not covered. For e.g., copper, the estimate (69′) amounts to 6 mrad.

In setting up the expressions for the electromagnetic fields inside a target of finite thickness, the reader might find the book by Ter-Mikaelian[17] helpful. The idea in constructing the fields is that the solution to the homogeneous Maxwell equations, $\mathbf{E}'$, appearing in Eq. (6), should be chosen such as to insure that the proper boundary conditions be fulfilled at each of now two target surfaces. Inside the target $\mathbf{E}'$ consists of two components, one, $\mathbf{E}'_+$, propagating forward (transmitted wave) and the other, $\mathbf{E}'_-$, propagating backwards (reflected wave). Being sufficient to consider normal incidence, it is straightforward, although a bit lengthy, to write up the equations for $\mathbf{E}'$. It turns out that inside the target we have in order of magnitude

$$E'_-/E'_+ \sim \max(|1-\epsilon|, \gamma^{-2}) . \tag{70}$$

Hence the component $\mathbf{E}'_-$ is negligible, cf. Secs. II B and II C. Further, the relative change of $\mathbf{E}'_+$ with respect to the expression for $\mathbf{E}'$ given, e.g., in Sec. II B, in order of magnitude is the square of the right-hand side of Eq. (70).

In total, we see that the actual target geometry introduces no changes in the photon intensities with respect to those derived for the specific case of normal incidence on a semi-infinite target.

III. COMPARISON WITH EXPERIMENTAL DATA

The conclusion of the detailed analysis of K-shell excitation by ultrarelativistic charged particles is that fairly accurate results are expected by application of the simple model [cf. Eqs. (1)–(4) and (8)]. Indeed, if the yield due to distant encounters in targets of atomic numbers $\gtrsim 10$ is computed as being due to the sum of the intensity given in the simple model, Eq. (1), and the small mixed intensity (43) with damping included, Eq. (63), the results obtained are correct within the overall accuracy of the applied theoretical method.

In order to compare our results with experimental data, Fig. 1, we need explicit expressions for the cross sections σ_γ^K and $d\sigma/dw$ entering Eqs. (4) and (8), respectively. For the former we apply the total photoelectric cross section $\sigma_\gamma^{\text{tot}}$ as tabulated by Veigele[20] and assume a simple scaling $\sigma_\gamma^K = \sigma_\gamma^{\text{tot}}(J_K-1)/J_K$, where $J_K \simeq 125/Z + 3.5$ is the K-jump ratio[20] for the element with atomic charge Ze. Interpolation between tabulated values is made through a linear fit to $\omega^3\sigma_\gamma$. Upon electron impact, the Møller expression[24] should be used for the differential cross section $d\sigma/dw$. With r_0 denoting the classical electron radius, $r_0 = e^2/mc^2$, Eq. (8) then leads to the result

$$\sigma_c = \frac{4\pi r_0^2}{\beta^2}\frac{mc^2}{\hbar\omega_K}\left\{1-w_I\left[1-\frac{1}{2}\left(\frac{\gamma-1}{\gamma}\right)^2 - \frac{2\gamma-1}{\gamma^2}\ln w_I\right]\right\} , \tag{71}$$

$$w_I \equiv \hbar\omega_K/mc^2(\gamma-1) ,$$

to first order in w_I. It should be noted that a factor of 2 has been included in Eq. (71) to account for the fact that each target atom appears with two K electrons. In the form (71), the cross section σ_c agrees with expressions as given by Tawara[25] (in Ref. 8 a minor misprint appears). For $\gamma \gtrsim 10$, the correction to 1 in large curlies in (71) is below 1%, except, perhaps, for the very heaviest elements, and σ_c is well approximated by the limiting value

$$\sigma_c \to \frac{4\pi r_0^2}{\beta^2}\frac{mc^2}{\hbar\omega_K} \simeq 1.00 \text{ barns} \times \frac{mc^2}{\hbar\omega_K} . \tag{72}$$

For positron impact one should use the Bhabha[24] rather than the Møller differential cross section, for heavier particle impact, the Mott cross section.[24] For high values of γ, the results for the contribution σ_c, Eq. (8), all approach the limiting value given in Eq. (72) (for the Mott cross section, cf. Ref. 26). However, also for moderate values of γ the differences encountered in the total K-shell excitation yield by changing between equal-velocity projectiles of, e.g., positrons, pions, and protons remain low, for $\gamma \sim 5$ smaller than $\sim 1\%$ (cf. also Ref. 10). We shall therefore use the electron result. We emphasize that through this construction the total K-shell excitation yield will be independent of spin and mass of the projectile. The yield depends only on the velocity, through the parameters β,γ. It is noted that for $Z_p^2 \neq 1$ an overall factor of Z_p^2 should be included.

The accuracy of the K-shell excitation cross sections obtained according to the above scheme has been checked against more elaborate theories. In the latter, density effects have been neglected corresponding to insertion of the intensity $dI^V/d\omega$ in Eq. (4). For $\gamma \gtrsim 10^2$, our results for, e.g., copper, are only $\simeq 10$ b, corresponding to $<3\%$, lower than those reported in Ref. 27 but 11–13 b, corresponding to $<3\%$, higher than those of Amundsen and Aashamar.[28] This is a fairly high accuracy in view of the rough procedure of dividing collisions into just two groups which represent opposite extremes. At low values of γ, our model is less accurate, leading to too high a cross section. For instance, for $\gamma \sim 5$, the result for copper is $\sim 7\%$ higher than those given in Refs. 27 and 28. In order to compare the relative data of Ref. 10 with theoretical predictions, as well as with earlier measurements, Fig. 1, we have therefore chosen to normalize both the latter to the cross section computed for 5 GeV/c protons by Amundsen and Aashamar.[28]

In Fig. 1 the solid and dashed curves represent the result of our model with and without inclusion of the density effect, i.e., the curves correspond to, respectively, the photon intensity $dI_0/d\omega$ of Eq. (30) and $dI^V/d\omega$ of Eq. (31). The data of experiments other than that of Ref. 10 fall close to the dashed curve (or, in some cases, even above, cf. Ref. 12). This is explained in our model by the fact that in those experiments the targets used were thin compared to the absorption length $\lambda_a(\omega)$, whereby the total photon intensity is close to the vacuum intensity [Eqs. (2) and (45)]. For instance, in the experiments of Ishii *et al.*[6] and Middleman *et al.*[4] copper foils of, respectively, 0.05 and 0.1–0.5 μm thickness were used. These numbers are very low compared to the absorption length which attains values $\lambda_a(\omega) \geq 3.8$ μm for $\omega \geq \omega_K$.

Figure 4 repeats the data and curves of Fig. 1. On the basis of the intensity (1) we have further produced the dot-dashed curve which corresponds to the conditions of the experiments reported in Refs. 10–11. Here the thickness of the copper foil was 25 μm which significantly exceeds $\lambda_a(\omega)$. In producing the curve we have taken into account selfabsorption of the outgoing K x rays which are observed at right angle to the target surface at the incidence side of the primary beam, which hits the foil at an angle of 45° to the surface normal. From the figure it is evident that the theory, even in its most simplified version, reproduces the experimental data very well.

IV. A FEW SCALING RELATIONS

For the sake of practical applications let us quote a few scaling relations. In general, the K-shell excitation yield depends on the ratio of the target thickness to the selfabsorption length of the outgoing K x rays, $\lambda_a(K_\alpha)$, and on the ratio of the latter to the absorption length for primary photons, $\lambda_a(\omega)$. For $\lambda_a(K_\alpha)/\lambda_a(\omega)$ we have by assumption of the approximate scaling $\sigma_\gamma^{\rm tot} \propto \omega^{-3}$, applying for $\omega > \omega_K$, the estimate

$$\frac{\lambda_a(K_\alpha)}{\lambda_a(\omega)} \simeq \frac{\lambda_a(K_\alpha)}{\lambda_a(\omega_K^+)} \left[\frac{\omega_K}{\omega}\right]^3 \simeq \left[\frac{125}{Z}+3.5\right]\left[\frac{\omega_K}{\omega}\right]^3 , \tag{73}$$

where the symbol ω_K^+ indicates the limiting value obtained at the top of the K edge. The last relation follows since the ratio in question for $\omega \rightarrow \omega_K +$ is given by the K-jump ratio, J_K. Due to the rapid decrease of $\sigma_\gamma^{\rm tot}$ with frequency, the contribution to the yield comes from a narrow range above ω_K and in a rough estimate we may therefore neglect the ω dependence in Eq. (73). As a result we see that $\lambda_a(K_\alpha)$ for all targets is several times longer than $\lambda_a(\omega)$. Consequently, with an x-ray detector mounted at the entrance side of a thick target, it is possible to look into the region where $dI'/d\omega$ and $dI^{\rm mix}/d\omega$ have been effectively quenched, that is, to regions where the density effect is dominant. On the other hand, for a target thicker than $\lambda_a(K_\alpha)$, an observer placed at the exit side will essentially only measure a yield corresponding to $dI_0/d\omega$—plus, of course, the close-encounter contribution.

For the contribution due to the mixed intensity, also the ratio of the formation length l to the damping length $2\lambda_a(\omega)$ is important. Since only γ values above γ_c are

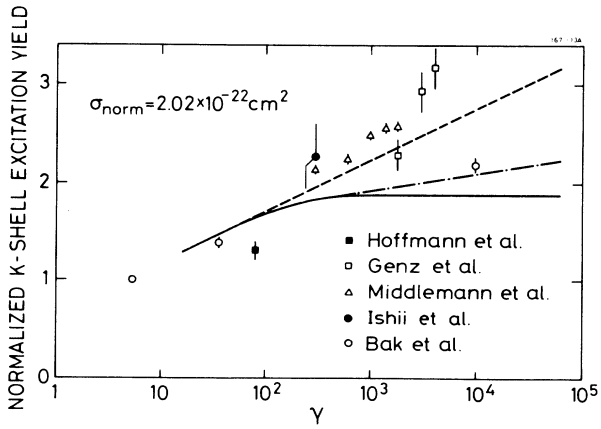

FIG. 4. Same as Fig. 1 but including the prediction for the experiment of Ref. 10 (dot-dash curve) obtained on the basis of the simple model [Eq. (1)].

of interest, we obtain

$$R_0 \equiv \frac{l}{2\lambda_a} = \frac{\omega c}{\lambda_a(\omega)\omega_p^2} \simeq R_0(\omega_K^+) \left[\frac{\omega_K}{\omega} \right]^2 . \quad (74)$$

Here the last approximation follows from the assumption of an ω^{-3} scaling of $\sigma_\gamma^{\rm tot}$. The quantity $R_0(\omega_K^+)$ attains the value

$$R_0(\omega_K^+) = 1.43 \times 10^{-5}\ {\rm keV}^{-1}\,{\rm b}^{-1}\ \hbar\omega_K \sigma_\gamma^{\rm tot}(\omega_K^+)/Z . \quad (75)$$

For hydrogenlike atoms the product $\hbar\omega_K \sigma_\gamma(\omega_K^+)$ is independent of the atomic number Z. In practice, some variation is observed. However, from the table of photo cross sections given by Veigele[20] we find

$$\hbar\omega_K \sigma_\gamma^{\rm tot}(\omega_K^+) \simeq 3 \times 10^5 {\rm keV\,b} , \quad (76)$$

the largest deviation for nongaseous elements with $Z \leq 35$ being 20%. The result (76) is also in good agreement with the one obtained for hydrogenlike atoms.[21] With Eq. (76) inserted in Eq. (75) we get

$$R_0(\omega_K^+) \simeq 4/Z . \quad (77)$$

Hence, except for the very lightest targets, the formation length is always short compared to the damping length for the mixed intensity.

A major interest in the relations (74) and (77) also stems from the fact that the size of the quantity R_0 provides information about the quality of the simple model. This is seen as the quantity R defined in Sec. II C equals the above R_0, except for a replacement of ω_p^2 by $\bar{\omega}_p^2$. In view of the result (77), it might therefore be necessary for the very lightest elements to use the full expressions, Sec. II C, for the photon intensities corresponding to the general dielectric function [Eq. (47)]. From the discussion in Sec. II C it is further recalled that for such targets the frequency region corresponding to $\epsilon_r > 1$,

$$1 \leq \omega/\omega_K \lesssim 1 + \tfrac{1}{2} e^{-Z/2} , \quad (78)$$

cf. Eq. (53), should not be neglected.

Among the remaining physical quantities, it is, of course, of special interest to establish a scaling relation with atomic number for the total yield. The close-collision contribution is in the limit of high-γ values given by Eq. (72). Since the virtual-photon intensity, Eq. (30), depends only logarithmically on ω whereas σ_γ^K scales roughly as ω^{-a} for $\omega > \omega_K$ with the exponent, a, attaining values in the vicinity of 3, the distant collision contribution may be estimated as

$$\sigma_d \simeq \frac{1}{a} \frac{dI}{d\hbar\omega}(\omega_K) \sigma_\gamma^K(\omega_K^+), \quad a \sim 3 . \quad (79)$$

For the ratio σ_d/σ_c we then obtain

$$\frac{\sigma_d}{\sigma_c} = \frac{2\alpha}{\pi a} L(\omega_K) \frac{\hbar\omega_K \sigma_\gamma^K(\omega_K^+)}{1.00\ {\rm barns} \times mc^2} \simeq 0.9 L(\omega_K) , \quad (80)$$

where the last result appears by the choice $a = 3$ and by application of the estimate (76). The quantity L is a suitable effective logarithmic factor attaining a value in the interval between the large square bracket factors of Eqs. (30) and (31). It typically is of the order of 10, i.e., distant collisions dominate. Since the ratio (80) is essentially Z independent, the total excitation yield scales roughly as σ_c,

$$Y = \left[1 + \frac{\sigma_d}{\sigma_c} \right] \sigma_c \simeq [1 + 0.9 L(\omega_K)]{\rm barns} \times \frac{mc^2}{\hbar\omega_K} . \quad (81)$$

For hydrogenlike atoms we get $Y \propto Z^{-2}$. As noted earlier, an overall factor of Z_p^2 should be included for projectiles of charge $Z_p e$.

For the last characteristic parameter of interest, namely, the critical γ value, γ_c, of Eq. (32), it is more difficult to find an approximate scaling relation since the atomic density and thereby the plasma frequency has no simple Z dependence. However, for solid elements $\hbar\omega_p$ remains within the range 15–90 eV, which means that within roughly a factor of 2 we have

$$\gamma_c^K \sim \frac{\hbar\omega_K}{40\ {\rm eV}} , \quad (82)$$

i.e., if we use ω_K corresponding to hydrogenlike atoms, the result is $\gamma_c^K \sim Z^2/3$.

V. CONCLUDING REMARKS

We have presented a comprehensive theoretical discussion of the dependence upon penetrated depth into a target of the K-shell excitation yield for ultrarelativistic charged-particle impact. In our description, due account is taken for target polarization and phenomena associated herewith, such as the density effect and the emission of transition radiation. A main result is that to a very good approximation the simple model, postulated earlier and discussed above, applies. By means of this model, all available experimental data have been explained. Thereby the so-called lack of the density effect mystery, which has persisted for a decade, is resolved. The model has further proven to stand all experimental tests—especially also a recent one, where extra foils producing transition radiation were included.[11] Besides exploring the validity of the simple model, the detailed discussion provides considerable insight into the underlying polarization phenomena. At shallow depths the interpretation of the depth dependence appears to be different from what is indicated by the simple model.

ACKNOWLEDGMENTS

The author wishes to acknowledge the inspiring collaboration with J. F. Bak, S. P. Møller, J. B. B. Petersen, E. Uggerhøj, and K. Østergaard, who performed the CERN experiments. I am also indebted to J. U. Andersen who continuously has shown interest in the work and kindly urged submission of this paper for publication.

*Present address: Institute of Physics, University of Aarhus, DK-8000 Århus C, Denmark.

[1]E. Fermi, Phys. Rev. **57**, 485 (1940).
[2]A. Crispin and G. N. Fowler, Rev. Mod. Phys. **42**, 290 (1970).
[3]G. R. Dangerfield, Phys. Lett. A **46**, 19 (1973).
[4]L. M. Middleman, R. L. Ford, and R. Hofstadter, Phys. Rev. A **2**, 1429 (1970).
[5]G. R. Dangerfield and B. M. Spicer, J. Phys. B **8**, 1744 (1975).
[6]K. Ishii *et al.* Phys. Rev. A **15**, 906 (1977).
[7]D. H. H. Hoffmann *et al.*, Z. Phys. A **293**, 187 (1979).
[8]M. Kamiya *et al.*, Phys. Rev. A **22**, 413 (1980).
[9]H. Genz *et al.*, Z. Phys. A **305**, 9 (1982).
[10]J. F. Bak *et al.*, Phys. Rev. Lett. **51**, 1163 (1983).
[11]J. F. Bak *et al.*, Phys. Scr. **33**, 147 (1986); **33**, 480(E) (1986).
[12]A. H. Sørensen and E. Uggerhøj, Comments At. Mol. Phys. **17**, 285 (1986).
[13]E. J. Williams, Mat.-Fys. Medd. Dan. Vidensk. Selsk. **13**, No. 4 (1935).
[14]J. D. Jackson, *Classical Electrodynamics* (Wiley, New York, 1975).
[15]A. H. Sørensen CERN Report No. CERN-EP187-25, 1987 (unpublished).
[16]G. M. Garibian, Zh. Eksp. Teor. Fiz. **33**, 1403 (1957) [Sov. Phys.—JETP **6**, 1079 (1958)].
[17]M. L. Ter-Mikaelian, *High-Energy Electromagnetic Processes in Condensed Media* (Wiley, New York, 1972).
[18]*Handbook of Mathematical Functions,* edited by M. Abramowitz and I. A. Stegun (Dover, New York, 1972).
[19]I. S. Gradshteyn and I. M. Ryzhik, *Table of Integrals, Series and Products* (Academic, New York, 1965).
[20]Wm. J. Veigele, Atomic Data **5**, 51 (1973).
[21]W. Heitler, *The Quantum Theory of Radiation* (Clarendon, Oxford, 1954).
[22]X. Artru, G. B. Yodh, and G. Mennessier, Phys. Rev. D **12**, 1289 (1975).
[23]G. M. Garibian, Zh. Eksp. Teor. Fiz. **38**, 1814 (1960) [Sov. Phys.—JETP **11**, 1306 (1960)].
[24]J. M. Jauch and F. Rohrlich, *The Theory of Photons and Electrons* (Addison-Wesley, Cambridge, 1955).
[25]H. Tawara in *Proceedings of the Tenth International Conference on the Physics of Electronic and Atomic Collisions, Paris,* 1977, edited by G. Watel (North-Holland, Amsterdam, 1978).
[26]F. Komarov, Radiat. Eff. **46**, 39 (1980).
[27]D. M. Davidovic and B. L. Moiseiwitsch, J. Phys. B **8**, 947 (1975); D. M. Davidovic, B. L. Moiseiwitsch, and P. H. Norrington, *ibid.* **11**, 847 (1978).
[28]P. A. Amundsen and K. Aashamar, J. Phys. B **14**, L153 (1981); and private communication.